IEEE Access
Multidisciplinary | Rapid Review | Open Access Journal

Received April 14, 2022, accepted April 22, 2022, date of publication April 25, 2022, date of current version May 4, 2022.

Digital Object Identifier 10.1109/ACCESS.2022.3170486

A Readout System for High Speed Interface of Wide Range Chemiresistive Sensor Array

SHANTHALA LAKSHMINARAYANA, (Graduate Student Member, IEEE), YOUNGHUN PARK, HYUSIM PARK, AND SUNGYONG JUNG, (Senior Member, IEEE)
Electrical Engineering Department, University of Texas at Arlington, Arlington, TX 76019, USA
Corresponding authors: Sungyong Jung (jung@uta.edu) and Hyusim Park (hyusim.park@mavs.uta.edu)

ABSTRACT This paper aims at designing a compact readout system for chemiresistive sensor array with high speed and high accuracy. The proposed scheme is based on Resistance-to-Voltage (R-V) conversion and targets high density wide ranged chemiresistive sensor, with input resistance range of 1 KΩ - 1 MΩ and 0.1% sensitivity. The proposed approach uses Adaptive Reference Resistor Tuning (ARRT) technique implemented with a digital variable potentiometer to achieve a high accuracy without sacrificing the dynamic range and the speed. The system is implemented on a printed circuit board with a microcontroller and a 16-bit Analog-to-Digital Converter (ADC), and it has a compact dimension of 10 cm × 6 cm, which is suitable for portable applications. The readout system works with a 5 V power supply, and the overall system power consumption is 150 mW. The system is designed to interface with a 118 sensor array and the experimental results achieved a satisfactory accuracy of 0.88%, as well as a measuring speed of 8.5 ms per sensor. Compared with existing approaches, our work targets a high density wide ranged chemiresistive sensor array and demonstrated high accuracy, high speed with the lowest circuit complexity, which is the novelty of this work.

INDEX TERMS Chemiresistive sensor, high density sensor array, microcontroller sensor interface, readout circuit, resistance-to-voltage conversion.

I. INTRODUCTION

Chemiresistive sensors have been widely investigated and used for toxic/harmful gas detection [1]–[3], environmental monitoring [4]–[6], food inspection [7]–[10] and various other applications [11] because of their merits such as simple sensing mechanism, cost effectiveness, and excellent sensitivity. The chemiresistor or chemiresistive sensor is a class of chemical sensor that changes its electrical resistance in response to chemical interaction between the sensing material and the target analyte. Thus, the purpose of a readout system is to convert the variation of target analytes into measurable electrical quantity such as voltage, current, and sometimes even time.

Different signal conditioning readout systems have been proposed to interpret response of chemiresistive sensors, which rely on conventional Resistance-to-Voltage (R-V) conversion using an Analog-to-Digital Converter (ADC) [12]–[20], Resistance-to-Time (R-T) conversion using RC oscillator and timer circuits [21]–[26], Direct Microcontroller Interface (DMI) [21]–[24], and quasi digital schemes namely, resistance to frequency, pulse width or period conversion [27]–[28].

The simplest method among them is the R-V conversion utilizing a voltage divider concept or a resistive DC excited Wheatstone bridge. However, in the case of detecting a wide range of sensor resistance such as chemiresistive gas sensors with dynamic variation up to 5 - 6 decades, this method cannot be employed due to its limitation of resistance range coverage [14]. Another strategy for R-V conversion is based on current excitation technique that forces a constant current through the sensor and measures the amplified output voltage [18]–[19], [29]–[31]. In this method, highly accurate and stable current reference sources are required to build the circuitry. Unfortunately, designing stable and precision current source is quite challenging because active components used in the circuitry are not linear. Also, the amplification section must be made programmable to adapt wide range, which increases the complexity, power, and size, without precision guarantee. While, the R-T scheme can measure wide resistive variation, but it requires two to four complete charging and discharging cycles to convert resistance

The associate editor coordinating the review of this manuscript and approving it for publication was Norbert Herencsar.

variation to time [21]–[26]. Consequently, the main drawback of R-T based approach is a long acquisition time when dealing with sensors having high base resistance. Hence, this solution is not suitable for readout system that requires a fast transient response from a high density sensor array with wide resistance range. The quasi digital system converts resistance to frequency, period, or pulse width variation; but another interface circuitry is necessary to covert the quasi digital output to digital, which makes the system complex [27]–[28]. In DMI technique, the microcontroller unit (MCU) excites a passive resistive [21]–[22] or capacitive [23] sensor and then measures the duration of the transient response to reach a predefined threshold using the embedded digital timer. Thus, no active electronic components are necessary between the sensor and the MCU, which minimizes the size, cost, and power consumption of the readout system. However, it also suffers from large processing time when dealing with wide range resistive sensor.

In recent era, there is a demand for high density sensor array to improve the selectivity and sensitivity of target analyte detection [32]–[34]. For instance, Electronic-Nose (E-Nose) is one of the cutting-edge applications which gained particular attention, that takes advantage of sensor diversity to mimic the human olfaction receptors [35]–[36]. Modern E-Nose system integrates different types of chemiresistive sensors in a single substrate to form a high density sensor array to enable multi analyte detection [35]. A variety of chemiresistive sensing materials, including conductive polymers, nanomaterials such as single and multi-wall carbon nanotubes (CNT), graphene, and nanoparticles can be deposited on the flexible substrate, using Inkjet or screen printing techniques to generate a high density sensor array with wide range [37]–[39]. However, it is hard to achieve fast, accurate, and low power system with the existing E-Nose readout systems; moreover, they are usually expensive and bulky [3], [5]–[7], [10].

Therefore, we propose an embedded readout system which can meet these requirements for a wide ranged high density chemiresistive sensor array, that can be used for applications like environmental monitoring, volatile organic compound (VOC) detection, toxic gas detection, and E-Nose. The target input resistance range of the proposed system is from 1 KΩ to 1 MΩ based on [35]. Since proposed system aims at a high density sensor array, the R-V conversion scheme with a voltage divider concept is selected due to low complexity and use of less active components, which leads to small form factor, low power consumption, and low cost. In order to accommodate wide ranged sensor while achieving high accuracy with this architecture, an Adaptive Reference Resistor Tuning (ARRT) technique with triple sampling method is employed to resolve limitation of conventional R-V. The proposed system shows an iterative improvement of the measurement accuracy and resolves the long measurement time problem of traditional R-T conversion method.

The rest of this paper is organized into following subsections. The first section introduces system design including hardware architecture and software design. The second section deals with an algorithm developed to improve the measurement accuracy and time. The last section presents experimental setup and results obtained using the proposed system.

II. SYSTEM DESIGN

A. READOUT SYSTEM SCHEME

The detailed block diagram of the proposed system is presented in Fig. 1, where S1 - S118 represents 118 number of chemiresistive sensor array. The system consists of a readout unit, control unit, and power management unit. The readout unit is embedded to convert chemiresistive sensor value to a quantifiable data, while control unit controls the readout unit, processes the obtained data from the readout unit, and transfers processed data to the user via Universal Serial Bus (USB). Lastly, the power management unit is implemented to provide a constant supply voltage to the system.

B. HARDWARE IMPLEMENTATION

The prototype of the proposed embedded system is implemented on a printed circuit board (PCB) using commercial off-the-shelf (COTS) components. "Eagle 9.4.2" software is used to design a 2-layer PCB as shown in Fig. 2.

Readout Unit: The objective of the readout unit is to digitize the resistance value of the target chemiresistive sensor (R_s), which consists of two electrodes. To establish the R-V conversion for quantification, one of the electrodes is connected to the reference resistor (R_{ref}) which is realized with a digital potentiometer (DPOT), while the other electrode is connected to constant supply voltage (V_{DD}) generated from power management unit as shown in Fig. 1. A Flexible Printed Circuit Board (FPCB) connector provides 120 contacts with 0.2 mm pitch to connect the 118 sensor array with the readout board. The remaining two contacts of the FPCB connector are utilized to provide V_{DD} to the sensor array. For addressing 118 different sensors individually, four 32 × 1 multiplexers are employed, which consumes low power of 100 μW and has low ON-resistance of 5.5 Ω which is negligible compared to R_s value. Commonly, the fixed value of R_{ref} in voltage divider circuit will induce voltage saturation at an ADC because of the nonlinearity in sensor response when dealing with wide resistance range. To avoid above mentioned problem, a dual channel 8-bit DPOT "AD5242BRZ1M" (Analog Devices) [41] having full scale error rate of ± 0.5 LSB is utilized to change the R_{ref} based on the value of R_s. A dual channel precision operational amplifier (OPAMP) is used as a buffer between the sensor and ADC, to avoid load impedance effects from high impedance source. The selected OPAMP provides low input offset voltage (V_{os}) of 5 μV and low input bias current of 0.2 pA to reduce output error [42]. Its output is converted to digital signal using an 8 channel 16-bit external ADC

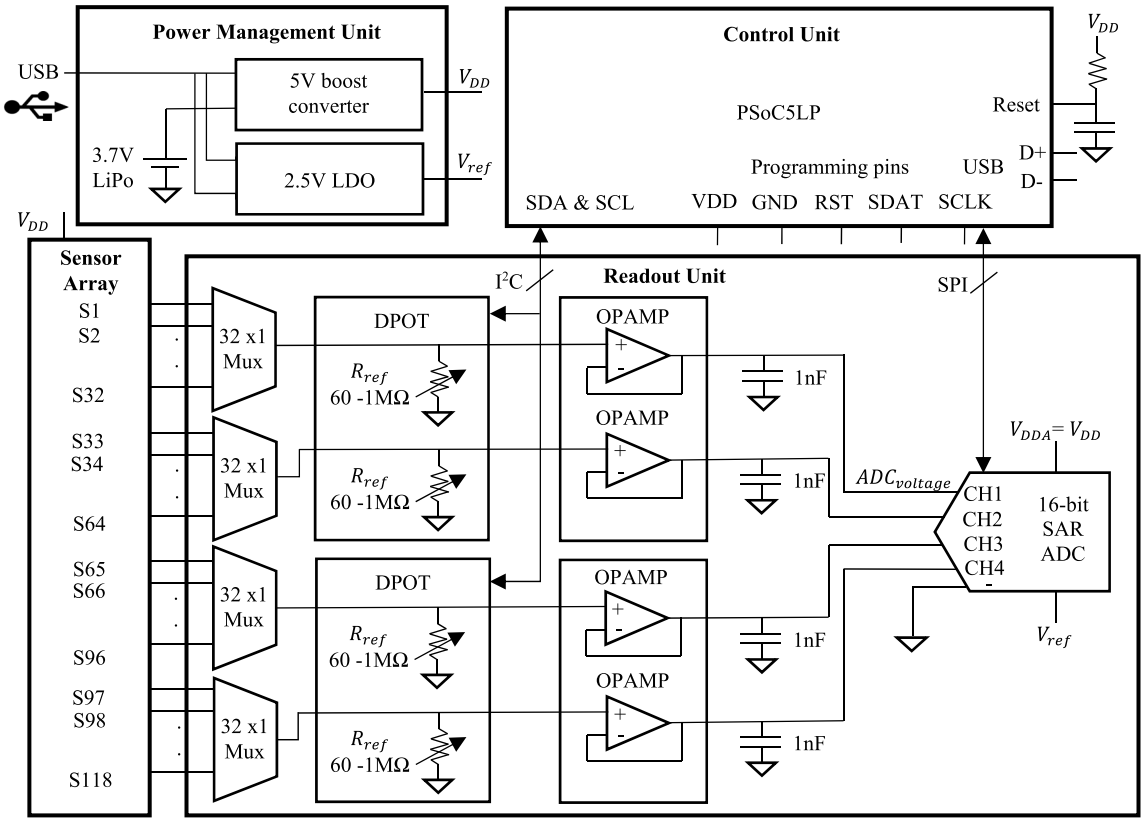

FIGURE 1. Detailed block diagram of the proposed system.

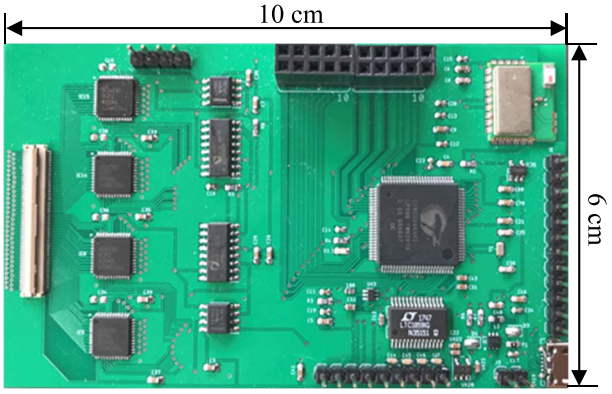

FIGURE 2. Prototype of readout system implemented on a PCB.

"LTC1859" (Analog Devices) [43] controlled by MCU using Serial Peripheral Interface (SPI). The ADC selection is a crucial step, as the ADC resolution affects the sensitivity of the sensor since the ADC should be able to detect the changes of the sensor output. The chosen ADC can identify voltage difference as small as 76 μV, which is able to detect 0.1 % variation of the sensor with resistance range between 1 KΩ and 1 MΩ (i.e.,1 Ω change for 1 KΩ base resistance and 1 KΩ change for 1 MΩ base resistance). The "LTC1859" uses a successive approximation algorithm and an internal sample-and-hold circuit to convert an analog signal to a 16-bit serial output respectively, providing an Integral Non Linearity (INL) of ± 3 LSB, Differential Non Linearity (DNL) of ± 2 LSB, and Signal to Noise Ratio (SNR) of 87 dB.

Once the ADC output voltage ($ADC_{voltage}$) is obtained, the unknown value of R_s can be calculated using voltage divider equation, as per (1).

$$R_s = \frac{R_{ref} \times (V_{DD} - ADC_{voltage})}{ADC_{voltage}} \tag{1}$$

Control Unit: The Programmable System-on-Chip (PSoC5LP) MCU is utilized as control unit [40]. This MCU provides a flexible configurable block of analog subsystem, digital subsystem, routing, and general purpose input/output pins (GPIO). The "PSoC5LP" architecture includes 32-bit Arm®Cortex®-M3 processor and operates with voltage range from 1.71 V to 5.5 V with ultra-low power consumption of 8.9 mA at 24 MHz, and 2 μA at sleep mode.

Power Management Unit: The readout board is designed to operate at a V_{DD} of 5 V. Power can be provided to the board either using a USB cable or a battery. A Type B micro-USB is used to power up the board and transmit the processed data to the personal computer (PC) using USB 2.0 standards. For providing a constant 5 V supply, a step-up or boost converter is employed, which can generate an output voltage of 5 V ± 2 % for an input voltage range of 2.3 V to 5.5 V with a supply current of 30 μA.

C. FIRMWARE & GUI DEVELOPMENT

To develop firmware for the readout board, following subsystems of "PSoC5LP" are utilized.

- Inter Integrated Circuit (I^2C) block to communicate with the DPOT
- SPI block to communicate with the ADC
- Control registers to control select lines of the 32×1 multiplexer
- USB block to control the USB 2.0 bus

The firmware of the MCU is written in embedded C programming language and is compiled using a "PSoC Creator 4.2" compiler released by Cypress semiconductors.

A customized Graphical User Interface (GUI) is developed to establish connection between the readout board and the PC using a USB Communication port (COM port). The GUI written in python provides a real time display plot to visualize the captured sensor data from the proposed device and saves the obtained sensor data in comma separated values (CSV) format file. "Tkinter" GUI framework and "matplotlib" library are utilized to build mentioned functionalities, meantime the USB communication is established using "pySerial" library. All the libraries are compiled into a single executable file using "pyinstaller" library.

III. PERFORMANCE EVALUATION

A. ACCURACY IMPROVEMENT BY ADAPTIVE REFERENCE RESISTOR TUNING

In conventional voltage divider method, the value of the R_{ref} is fixed to either most likely occurring value of R_s in the range or the median value of the R_s range (R_{mid}) [14], [22]. The conventional method is also referred as a single point calibration method and cannot be applied for measurement of the wide ranged sensor because of nonlinearity problem. Let us consider a chemiresistive sensor with sensor resistance R_s that varies with respect to gas concentration as in (2),

$$R_s = A \times C^{-\alpha} \tag{2}$$

where, C is the gas concentration in ppm, A and α are constants set as 1×10^6 and 1 respectively, for the simulation in Fig. 3 [7]. Using (1) and (2), (3) can be derived.

$$ADC_{voltage} = \frac{V_{DD} \times R_{ref}}{R_{ref} + (A \times C^{-\alpha})} \tag{3}$$

Fig. 3 shows the graph of $ADC_{voltage}$ versus gas concentration (considering 0 to 1000 ppm as an example) utilizing (3), when $R_{ref} = R_{mid}$ in conventional R-V method. The graph indicates a rapid rise in response at lower gas concentrations and the slowing of response at higher gas concentrations (voltage saturation). When $R_{ref} \ll R_s$ (at low gas concentration), denominator term $R_{ref} + (A \times C^{-\alpha})$ reduces to $(A \times C^{-\alpha})$, which gives a fairly linear relationship between the $ADC_{voltage}$ and the gas concentration C. But, when $R_{ref} \gg R_s$ (at high gas concentration), R_{ref} will start to dominate the $R_{ref} + (A \times C^{-\alpha})$ term, and the corresponding change in $ADC_{voltage}$ to gas concentration becomes saturated.

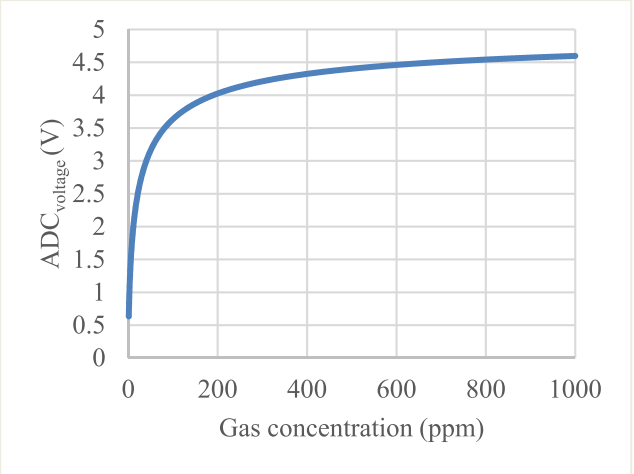

FIGURE 3. ADC response versus gas concentration in conventional R-V method using fixed R_{ref}.

To cope with mentioned nonlinearity problem due to single point calibration with fixed R_{ref}, ARRT technique is realized with a DPOT, which can alter the R_{ref} to 256 distinct values, so that R_{ref} can be automatically balanced to value of R_s. Thus, the condition $R_{ref} \approx R_s$ is always maintained to achieve $ADC_{voltage} \approx \frac{V_{DD}}{2}$ for avoiding the voltage saturation problem at higher gas concentration, thus helps to achieve high linearity throughout the measurement range. To adjust the R_{ref} to match with R_s, an iterative setting algorithm with triple sampling is developed and embedded in the MCU firmware. The value of DPOT which indicates R_{ref}, is regulated in three consecutive iterations. Each iteration back calculates the R_s using (1) with obtained $ADC_{voltage}$ while changing the DPOT values as per (4). At the first iteration, the system calculates the R_s value by setting R_{ref} to R_{mid}, which is same as conventional method. In the second and third iterations, the R_{ref} value is set to calculated value of R_s obtained in the previous iteration to tune the value of R_{ref} close enough to actual R_s. For the sensor array, each sensor data is sampled and processed with the iterative setting algorithm repeatedly until all sensor data is obtained. This methodology iteratively improves the accuracy, at the expense of increased measurement time. However, a timing enhancement scheme is explored to compensate for the measurement time, which is explained in section III-C.

The resistance value of the DPOT can be varied from 60 Ω - 1 MΩ by programming registers. The DPOT has 3 terminals, 'A' & 'B' are the end terminals and 'W' is the wiper terminal. The wiper position of DPOT is programmed by an I^2C serial data interface and can be set to 256 different positions. The resistance value of the DPOT (R_{DPOT}) can be set and calculated using the formula (4).

$$R_{DPOT} = R_{ref} = R_{WA}(D) = \frac{256 - D}{256} \times R_{AB} + R_W \tag{4}$$

where, R_{WA} is the resistance between DPOT 'A' terminal and the wiper terminal, and D is the decimal equivalent of

the binary code between 0 and 255 which is loaded in the 8-bit register of DPOT [41]. R_{AB} is the nominal end-to-end resistance that is 1 MΩ while R_W is the wiper resistance contributed by ON resistance of the internal switch which is 60 Ω.

B. READOUT RESOLUTION IMPROVEMENT BY ADAPTIVE REFERENCE RESISTOR TUNING

Another important parameter to consider for an evaluation of the system is the resolution corresponding to variation of the sensor resistance value, due to the changes in target gas concentration. As response to variation in the target gases, the variation of the sensor resistance (R_s') can be specified as $R_s' = R_s + \Delta R_s$. The proposed system targets a sensor with sensitivity of ± 0.1 %. Thus, R_s' can be considered as $0.009R_s$ or $1.001R_s$.

Let us denote $V_{(nogas)}$ as $ADC_{voltage}$ in (1) without target gas exposure and $V_{(gas)}$ indicates $ADC_{voltage}$ as per (1) in condition where sensor is exposed to gas in conventional R-V method, where R_{ref} is fixed to R_{mid}. The term of $\Delta V = V_{(nogas)} - V_{(gas)}$ stipulates the $ADC_{voltage}$ change due to target gas variation and is derived in (7) using (5) and (6).

$$V_{(nogas)} = \frac{V_{DD}\left(\frac{R_{max}+R_{min}}{2}\right)}{\left(\frac{R_{max}+R_{min}}{2}\right)+R_s} \tag{5}$$

$$V_{(gas)} = \frac{V_{DD}\left(\frac{R_{max}+R_{min}}{2}\right)}{\left(\frac{R_{max}+R_{min}}{2}\right)+(R_s+\Delta R_s)} \tag{6}$$

$$\Delta V \approx \frac{0.002\times V_{DD}\,(R_{max}+R_{min})\,R_s}{(R_{max}+R_{min}+2.001R_s)^2} \tag{7}$$

where $R_s' = 1.001R_s$. The ΔV can be calculated using (7) which ranges from 9.95 μV to 1.11 mV, considering the target chemiresistive sensor R_s ranges between R_{min} and R_{max} of 1 KΩ − 1 MΩ, and V_{DD} as 5 V. The minimum voltage of ΔV is 9.95 μV which cannot be detected from 16-bit ADC since it has a 76 μV resolution. Therefore, it requires a higher bit ADC that is very expensive and not easily accessible. The conventional method not only suffers from higher bit ADC requirement, but also noise issue since 9.95 μV is very small signal that can be easily distorted. Thus, accommodating sensor with ± 0.1 % sensitivity using the conventional method is neither possible nor efficient.

Similarly, ΔV of proposed method with the ARRT technique can be written as (10) which sets $R_{ref} \cong R_s \pm R_{step}$ after three iterations, considering the step size of DPOT (R_{step}).

$$V_{(nogas)} = \frac{V_{DD}\times(R_s \pm R_{step})}{(R_s \pm R_{step}) + R_s} \tag{8}$$

$$V_{(gas)} = \frac{V_{DD}\times(R_s \pm R_{step})}{(R_s \pm R_{step}) + (R_s + \Delta R_s)} \tag{9}$$

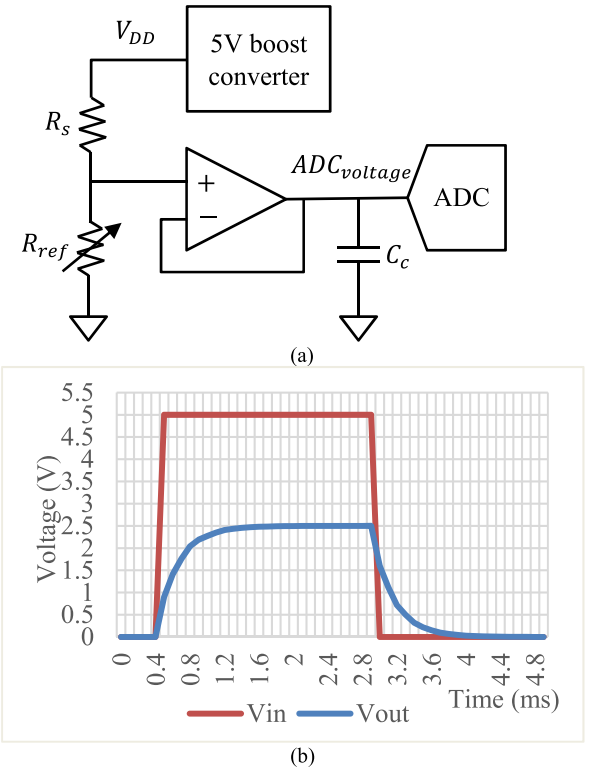

FIGURE 4. (a) Simplified readout circuit, (b) Timing diagram.

$$\Delta V \approx \frac{0.001\times V_{DD}\left(R_s \pm R_{step}\right)R_s}{\left(2.0005R_s \pm R_{step}\right)^2} \tag{10}$$

where, R_{step} of the selected DPOT is 3.9 KΩ calculated as per (4). The ΔV calculated using (10) ranges from 0.7 mV to 1.24 mV for the measurement range 1 KΩ - 1 MΩ and can be easily detected by 16-bit ADC. Thus, proposed method can be used for the measurement system of chemiresistive sensor with ± 0.1 % sensitivity with high accuracy.

C. TIMING IMPROVEMENT BY MUX SELECTION SCHEME

A simplified readout circuit and a corresponding timing diagram of proposed system is depicted in Fig. 4. It consists of a voltage divider circuit embodied with R_s, R_{ref}, buffer, ADC, and decoupling capacitor (C_c). The C_c at ADC input is implemented to reduce the interference generated from power supply fluctuations. At any time, when an input voltage V_{in} which has an amplitude of V_{DD} is applied to R_s, the $ADC_{voltage}$ can be determined based on the values of R_{ref} and R_s, which is denoted as V_{out} in the timing diagram. To extract the proper ADC output, a settling time (t_{set}) at the ADC input is required, which takes at least a time of 5T [22]; where T is the time constant for parallel RC circuit given by,

$$T = (R_{ref}||R_s)\times C_c. \tag{11}$$

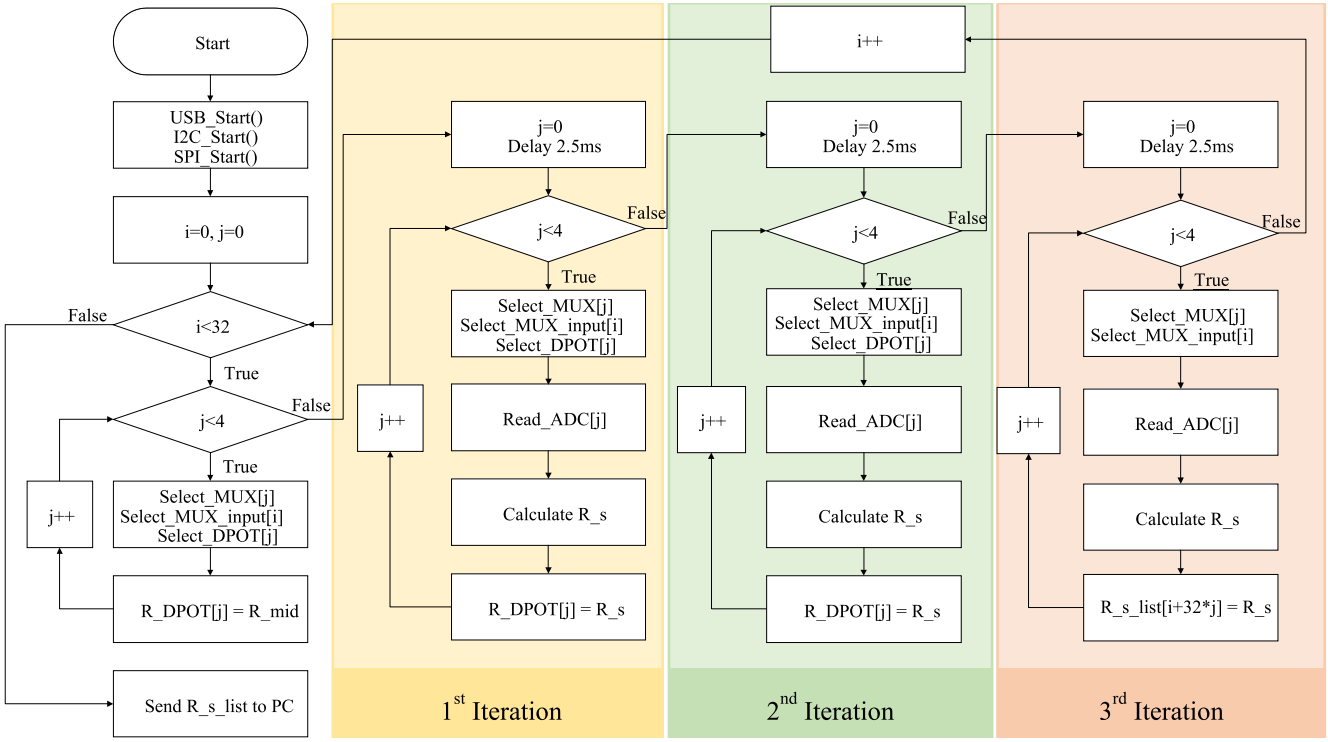

FIGURE 5. Flow chart of the proposed method.

Hence, the required t_{set} can be calculated as,

$$t_{set} = 5(R_{ref}||R_s) \times C_c. \tag{12}$$

The maximum time of t_{set} arises for a combination of R_s and R_{ref} equals to 1 MΩ (i.e., 5 × (1 MΩ|| 1 MΩ) × 1 nF = 2.5 ms), where the C_c is set to optimal value of 1 nF sufficient to avoid the supply fluctuations meanwhile reducing the delay time. The settling time in unity-gain feedback of the OPAMP used in the design is 1.6 μs [42] which is negligible compared to the settling time of 2.5 ms calculated using (12) and thus can be neglected.

The total processing time (T_{tot}) can be acquired as,

$$T_{tot} = t_{acq} + t_{conv} + t_{MCU} \tag{13}$$

where, t_{acq} is the sensor acquisition time which depends on the value of t_{set}, t_{conv} is the ADC conversion time (4 μs from LTC1859), and t_{MCU} is the MCU processing time needed to set the DPOT value via I^2C, perform arithmetic operations, and transferring the obtained data to GUI. Since triple sampling is employed in the proposed scheme, 3 × t_{set} is necessary which is 7.5 ms to measure each sensor. Therefore, if all of 118 sensors in the array are processed in order, t_{acq} will be 7.5 ms × 118 = 885 ms. Fig. 5 represents the flowchart of proposed method. The proposed architecture uses four different readout channels with a 32 × 1 MUX, a DPOT, an OPAMP, and an ADC, respectively. In the flow chart, '*j*' variable represents four readout channels, and '*i*' variable indicates 32 inputs of MUX. Once the system initialization is complete, the R_s value is read by tuning R_{ref} in three consecutive iterations as explained in section III-A.

To reduce the time t_{acq}, mux selection scheme is utilized where 118 sensor data is acquired channel by channel, instead of reading in series. As first step, the select lines of all four MUXs are set by the MCU such that first mux input ($i = 0$) is selected. During second step, DPOT value is set for all four channels and a delay of 2.5 ms is given as t_{set}. Thus, in a span of 2.5 ms, $ADC_{voltage}$ of all four channels are settled down and ADC can digitize the voltage accurately. Since triple sampling is employed, above steps are repeated during 2nd and 3rd iterations by tuning DPOT. This is followed by incrementing the '*i*' value until all 32 mux inputs are acquired. As a result, t_{acq} for 118 sensors is reduced to a value 7.5 ms × 32 = 240 ms. It is demonstrated in experiment that the overall measurement time is 1.01 s to collect, process, and transfer the data of 118 sensors to GUI. This implies a measurement speed of 8.5 ms to read each sensor output including the t_{conv} and the t_{MCU}.

IV. EXPERIMENTAL SETUP & RESULTS

The proposed system is tested electrically for verification. To represent 118 chemiresistive sensor array, an electrical equivalent model consisting of 118 resistor array is fabricated on a PCB. It is realized by 0.1 % tolerance thin film discrete resistors, where resistance varied from 1 KΩ to 1 MΩ. The 118 resistor array is connected to the designed readout board using FPCB jumper cable. The USB cable is utilized to

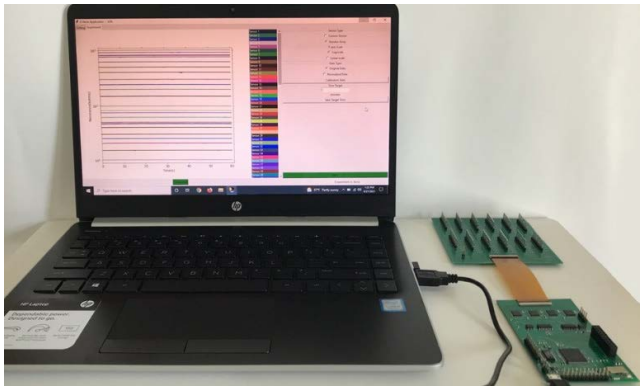

(a)

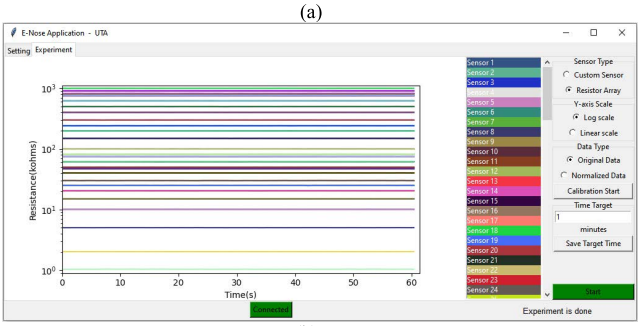

(b)

FIGURE 6. (a) Photo of test setup, (b) 118 resistor array readings displayed in GUI.

TABLE 1. Measurement readings comparison between fixed reference resistor and adaptive reference resistor tuning.

R_{exp}(KΩ)	R_{meas}(KΩ)		*Error* (%)		*Fluctuation* (%)	
Exp	CM	PM	CM	PM	CM	PM
10	15.89	10.08	-58.87	-0.76	16.81	0.33
15	20.98	15.13	-39.86	-0.88	14.23	0.38
49.9	54.71	49.81	-9.64	0.19	4.15	0.50
100	103.96	99.43	-3.96	0.57	2.19	0.30
300	301.44	299.17	-0.48	0.28	0.77	0.54
499	500.79	498.06	-0.35	0.19	0.79	0.35
750	747.53	751.78	0.33	-0.24	0.86	0.47
806	803.48	807.56	0.31	-0.19	0.93	0.52
909	900.23	906.68	0.96	0.26	0.73	0.46
1000	990.39	999.04	0.96	0.10	1.18	0.42

connect readout board and PC, to power up the board, and to display the obtained data in customized GUI as shown in Fig. 6. (a). In the GUI, resistance values of 118 sensors are displayed, which varies with respect to time. The GUI provides the option to select and monitor individual sensor in the array and each sensor result is saved in the CSV format file to record the sensor response. Fig. 6. (b) shows the output of 118 sensors displayed in the GUI, which corresponds to the resistance values in the 118 resistor array PCB.

Using the experimental setup in Fig. 6. (a), 118 resistor array values are measured using both conventional

TABLE 2. System performance summary.

Input resistance range	1 KΩ - 1 MΩ
Sensitivity	± 0.1 %
Number of sensors in array	118
Measurement speed	8.5 ms / sensor
Measurement time for 118 sensors	1.01 s
Worst-case error	0.88 %
Supply voltage	5 V
Power consumption	150 mW @5 V
ADC resolution	16-bits
Device dimension	10 cm × 6 cm

method (CM) where R_{ref} is fixed to R_{mid} and the proposed method (PM) with ARRT technique. Table 1 shows the comparison results between two methods, where Error (%) provides insight on the deviation in the measured resistance value (R_{meas}) compared to expected resistance value (R_{exp}). The Fluctuation (%) informs about the difference in the maximum measured resistance and minimum measured resistance with respect to R_{exp}, when same resistance is measured multiple times in one hour.

From the TABLE 1, it is evident that the CM showed huge error rates especially for smaller sensor resistance, whereas the PM showed worst-case error of 0.88 %. These variations were caused by the combination of the supply voltage fluctuation of regulators by 5 V ± 2 %, DPOT full scale error of ± 0.5 % LSB, step size limitations of DPOT due to 8-bit, offset voltage of the OPAMP, 0.1 % tolerance of thin-film discrete resistors in the resistor array, and the ADC conversion error. The overall system performance is summarized in Table 2.

The Fig. 7 illustrates the error analysis and linearity test result of the CM and PM. The linearity test is performed by comparing R_{exp} with R_{meas} throughout the target measurement range. In CM, the absolute minimum error rate occurs when $R_s \approx R_{mid}$ (at 500 KΩ) and increases as R_s moves away from R_{mid}. In contrast, the PM proves that the measured results have close correlation with the expected value with a worst-case error less than 0.88 %. Also, the CM showed a non-linearity in the results when $R_s \ll R_{ref}$. However, PM showed the linear response throughout wide range of sensor resistance value, varied from 1 KΩ to 1 MΩ.

The comparison of proposed readout scheme with recent existing methodologies is presented in Table 3. Compared to R-T conversion scheme in [21]–[26], proposed system can afford a wide range. In [21]–[26], as the sensor base resistance increases, the conversion time also increases proportionally due to the charging and discharging time. Although [27]–[28] offers a wide input range, the proposed system demonstrated a significantly better measurement time and accuracy. Compared to the R-V techniques realized in [12]–[20], the

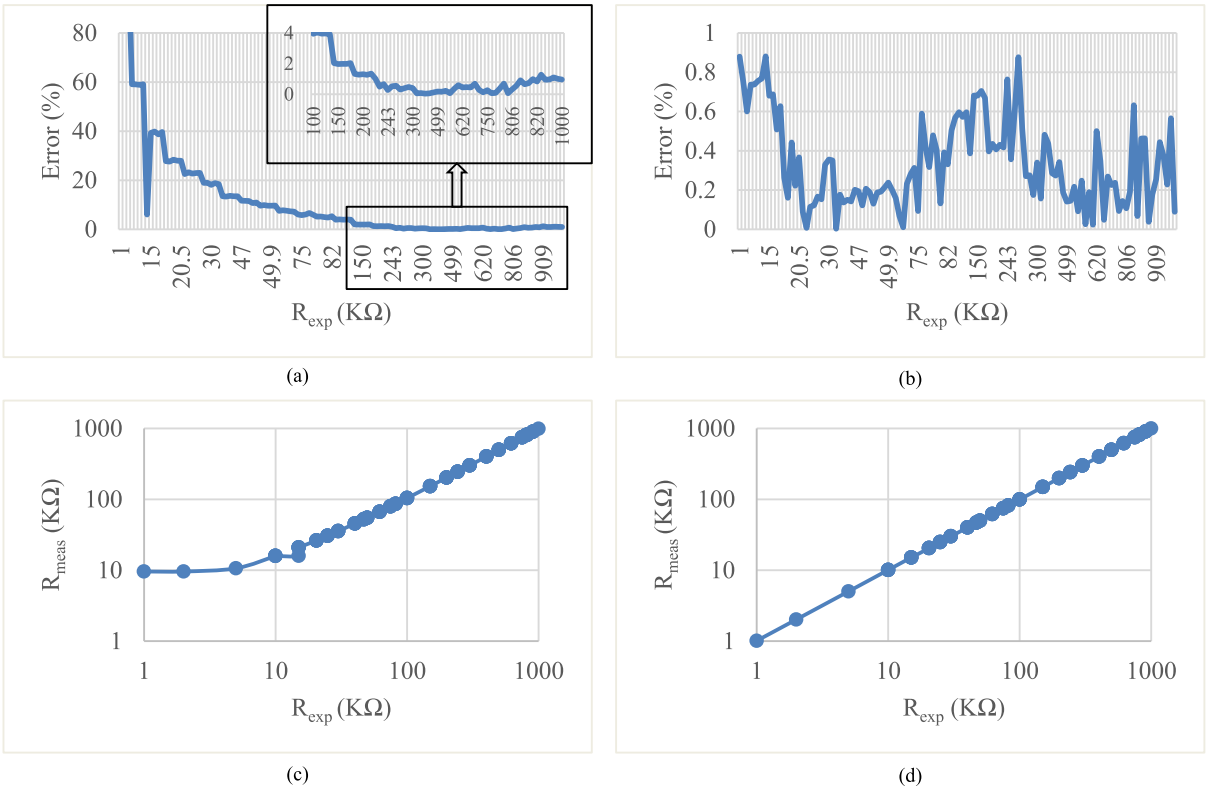

FIGURE 7. (a) and (b): Error rate of CM and PM respectively, (c) and (d): Linearity test result of CM and PM respectively, in log scale.

TABLE 3. Performance comparison of existing chemiresistive sensor readout schemes with proposed system.

Ref	Conversion Principle	Number of sensors	Sensor Range (Ω)	Error (%)	Measurement time per sensor (s)	Microcontroller	Year
This work	Resistance to Voltage	118	1 K –1 M	0.88	8.5 m	PSoC5LP	2022
[12]	Resistance to Voltage	10 × 10	2 K – 20 K	<0.61	NA	MSP430F5418A	2015
[13]	Resistance to Digital	1	1 K – 1 M	<0.05	96 m @ Rx=1 KΩ	ATmega328	2017
[14]	Resistance to Voltage	1	100	NA	25.8 m	ATmega32A4	2016
[15]	Resistance to Voltage	1	10 – 8 M	2	NA	Not used	2013
[16]	Resistance to Voltage	1	100 - 10 M	1.5	NA	Not used	2012
[17]	Resistance to Voltage	1	20 K - 1.1 M	0.78	NA	Not used	2020
[18]	Resistance to Voltage	1	1 K - 0.5 M	1	NA	MSP430F5529	2020
[19]	Resistance to Voltage	3	1 K - 1 M	1	NA	MSP430F5529	2022
[20]	Resistance to Voltage	60	1 K - 1 M	2.5	19.6 m	PSoC5LP	2022
[21]	Resistance to Time	1	100 - 150	0.12	2.58 m	Atmega328P	2020
[22]	Resistance to Time	1	100 - 146.2	0.06	5.3 m	ATmega328	2017
[23]	Resistance to Time	1	50 – 800 K	0.91	5 m	ATmega328	2021
[24]	Resistance to Time	1	1000 - 1100	0.33	NA	ATmega328	2014
[25]	Resistance to Time	28	100 - 16.2 K	0.88	1.1 m	FPGA	2021
[26]	Resistance to Time	1	1 K - 3 K	1	8.5	Arduino Uno	2020
[27]	Resistance to Frequency	17	200 - 10 M	1	1	Mini STM32	2021
[28]	Resistance to Period	1	820 K - 9.1 M	4	NA	Not used	2015

proposed system showed comparable performance in accuracy with a high speed and compact architecture, which is critical to design an embedded readout system for large sensor array. Our previous work, [20] is targeting the wearable

application; thus, the critical performance criteria were small form factor and low power consumption. So that, the accuracy and speed were compromised in the previous work which were 2.5 % and 19.6 ms per sensor, respectively. However, in this work, the MCU firmware is significantly modified to improve the accuracy by implementing a new technique, which is the ARRT with triple sampling. Apart from that, a mux selection scheme is embedded in the MCU, that aided in improving the measurement speed. In spite of adopting a higher density array from 60 to 118, the measurement speed and accuracy were improved substantially compared to the previous work.

Overall, the proposed system achieves the finest optimal result in terms of accuracy, input resistance range, and the measurement speed. To summarize, the salient features of the proposed system which makes the system unique from existing methodologies are as follows: The system can achieve a wide measurement range of 1 KΩ - 1 MΩ and the novel ARRT with triple sampling technique implemented using MCU firmware accomplished a high accuracy with worst-case error rate of 0.88 %. The system accommodates a high density sensor array up to 118 sensors and simultaneous measurement can be performed, leading to a high speed sensor interface. The prototype achieved a measure time of merely 8.5 ms per sensor, for a 1 MΩ resistance calculation, equivalent to a 117 Hz sampling speed. This result is significantly faster than the existing works that target a wide measurement range. Nevertheless, the system automatically tunes the reference resistor to enhance the sensitivity of resistance measurement. The auto tuning provides a flexibility to adjust the DPOT value to sensor resistance value, which avoids the ADC saturation and achieves wide range measurement.

V. CONCLUSION

In this work, a readout system suitable for the high density chemiresistive sensor array in the range of 1 KΩ - 1 MΩ is presented. A customized GUI is developed to control the system, display the results, and save the data in the PC. The designed readout is embedded with the R-V conversion methodology using MUX, DPOT, ADC, and the MCU, providing a compact solution for portable applications, which target high density chemiresistive sensor array to detect variety of analytes. To enhance the sensor resistance range of conventional R-V conversion method, we proposed the R-V conversion with the ARRT and triple sampling technique. As a result, the proposed readout system can measure wide ranged chemiresistive sensor with relatively high accuracy, where the worst-case error rate is 0.88 %. The readout system also offers a high speed sensor interface with a measurement time of only 8.5 ms per sensor. Compared to existing chemiresistive sensor readout topologies, the proposed system yields a magnificent optimal result in terms of the measurement speed, input resistance range, and accuracy. The system is implemented on a PCB with a compact dimension of 10 cm × 6 cm and suitable for a mass production at low cost. The key applications for the proposed embedded system are toxic gas detection, indoor and outdoor air quality monitoring, comprehensive breathing analyzers, VOC detection system, portable E-Nose etc. The target resistance range of 1 KΩ - 1 MΩ covers majority of the chemiresistive gas sensors that are used in the listed applications. The future work includes testing the prototype with actual sensors integrated to the readout system and to detect the target analytes of various concentrations.

REFERENCES

[1] A. Holovatyy, "Development of arduino-based embedded system for detection of toxic gases in air," in *Proc. IEEE 13th Int. Sci. Tech. Conf. Comput. Sci. Inf. Technol. (CSIT)*, 2018, pp. 139–142.
[2] C. K. Joshi and S. Jugran, "Design and developement of an embedded based device for the detection of toxic gases with raspberry Pi," in *Proc. Int. Conf. Adv. Comput., Commun. Mater. (ICACCM)*, Aug. 2020, pp. 437–442.
[3] S. Sadeghifard and L. Esmaeilani, "A new embedded e-nose system to identify smell of smoke," in *Proc. 7th Int. Conf. Syst. Syst. Eng. (SoSE)*, Jul. 2012, pp. 253–257.
[4] Y. W. Kim, S. J. Lee, G. H. Kim, and G. J. Jeon, "Wireless electronic nose network for real-time gas monitoring system," in *Proc. IEEE Int. Workshop Robotic Sensors Environ.*, Nov. 2009, pp. 169–172.
[5] F. C. Tian, C. Kadri, L. Zhang, J. W. Feng, L. H. Juan, and P. L. Na, "A novel cost-effective portable electronic nose for indoor-/in-car air quality monitoring," in *Proc. Int. Conf. Comput. Distrib. Control Intell. Environ. Monitor.*, Mar. 2012, pp. 4–8.
[6] P. Strobel, A. Lfakir, M. Siadat, and M. Lumbreras, "A portative gas recognition system based on metal oxide gas sensor array," in *Proc. IEEE Sensors*, Oct. 2006, pp. 123–126.
[7] A. Das, T. K. Ghosh, A. Ghosh, and H. Ray, "An embedded electronic nose for identification of aroma index for different tea aroma chemicals," in *Proc. 6th Int. Conf. Sens. Technol. (ICST)*, Dec. 2012, pp. 577–582.
[8] M. Abdelkhalek, S. Alfayad, F. Benouezdou, M. B. Fayek, and L. Chassagne, "Compact and embedded electronic nose for volatile and non-volatile odor classification for robot applications," *IEEE Access*, vol. 7, pp. 98267–98276, 2019.
[9] A. H. Abdullah, A. H. Adom, A. Y. M. Shakaff, M. N. Ahmad, A. Zakaria, F. S. A. Saad, C. M. N. C. Isa, M. J. Masnan, and L. M. Kamarudin, "Hand-held electronic nose sensor selection system for basal stamp rot (BSR) disease detection," in *Proc. 3rd Int. Conf. Intell. Syst. Modeling Simulation*, Feb. 2012, pp. 737–742.
[10] A. Kumbhar, D. C. Gharpure, B. A. Botre, and S. S. Sadistap, "Embedded e-nose for food inspection," in *Proc. 1st Int. Symp. Phys. Technol. Sensors (ISPTS)*, Mar. 2012, pp. 311–314.
[11] G.-J. Jong, Hendrick, Z.-H. Wang, K.-S. Hsieh, and G.-J. Horng, "A novel feature extraction method an electronic nose for aroma classification," *IEEE Sensors J.*, vol. 19, no. 22, pp. 10796–10803, Nov. 2019.
[12] L. Shu, X. Tao, and D. D. Feng, "A new approach for readout of resistive sensor arrays for wearable electronic applications," *IEEE Sensors J.*, vol. 15, no. 1, pp. 442–452, Jan. 2015.
[13] V. Sreenath, K. Semeerali, and B. George, "A resistive sensor readout circuit with intrinsic insensitivity to circuit parameters and its evaluation," *IEEE Trans. Instrum. Meas.*, vol. 66, no. 7, pp. 1719–1727, Jul. 2017.
[14] Z. Czaja, "An implementation of a compact smart resistive sensor based on a microcontroller with an internal ADC," *Metrol. Meas. Syst.*, vol. 23, no. 2, pp. 225–238, 2016.
[15] A. De Marcellis, G. Ferri, and P. Mantenuto, "A novel 6-decades fully-analog uncalibrated Wheatstone bridge-based resistive sensor interface," *Sens. Actuators B, Chem.*, vol. 189, pp. 130–140, Dec. 2013.
[16] A. De Marcellis, G. Ferri, and P. Mantenuto, "Analog Wheatstone bridge-based automatic interface for grounded and floating wide-range resistive sensors," *Sens. Actuators B, Chem.*, vol. 187, pp. 371–378, Oct. 2013.
[17] K. Kishore, S. Malik, M. S. Baghini, and S. A. Akbar, "A dual-differential subtractor-based auto-nulling signal conditioning circuit for wide-range resistive sensors," *IEEE Sensors J.*, vol. 20, no. 6, pp. 3047–3056, Mar. 2020.
[18] M. Ahmad, S. Malik, S. Dewan, A. K. Bose, D. Maddipatla, B. B. Narakathu, M. Z. Atashbar, and M. S. Baghini, "An auto-calibrated resistive measurement system with low noise instrumentation ASIC," *IEEE J. Solid-State Circuits*, vol. 55, pp. 3036–3050, 2020.

[19] M. Ahmad, S. Malik, H. Patel, and M. S. Baghini, "A portable low-voltage low-power ppm-level resistive sensor measurement system," *IEEE Sensors J.*, vol. 22, no. 3, pp. 2338–2346, Feb. 2022.

[20] S. Lakshminarayana, Y. Park, H. Park, and S. Jung, "High density resistive array readout system for wearable electronics," *Sensors*, vol. 22, no. 5, p. 1878, Feb. 2022.

[21] R. Anandanatarajan, U. Mangalanathan, and U. Gandhi, "Enhanced microcontroller interface of resistive sensors through resistance-to-time converter," *IEEE Trans. Instrum. Meas.*, vol. 69, no. 6, pp. 2698–2706, Jun. 2020.

[22] P. R. Nagarajan, B. George, and V. J. Kumar, "Improved single-element resistive sensor-to-microcontroller interface," *IEEE Trans. Instrum. Meas.*, vol. 66, no. 10, pp. 2736–2744, Oct. 2017.

[23] L. Areekath, B. George, and F. Reverter, "Analysis of a direct microcontroller interface for capacitively coupled resistive sensors," *IEEE Trans. Instrum. Meas.*, vol. 70, pp. 1–10, 2021.

[24] R. N. Ponnalagu, G. Boby, and V. J. Kumar, "A microcontroller sensor interface suitable for resistive sensors with large lead resistance," *Int. J. Smart Sens. Intell. Syst.*, vol. 7, no. 5, pp. 1–5, Jan. 2014.

[25] J. A. Hidalgo-Lopez, O. Oballe-Peinado, J. Castellanos-Ramos, J. C. Tejero-Calado, and F. Vidal-Verdu, "Wide range calibration method for direct interface circuits and application to resistive force sensors," *IEEE Sensors J.*, vol. 21, no. 20, pp. 22956–22966, Oct. 2021.

[26] D. Hunasekattte, "A Resistance-to-time convertor to enhance resistive sensitivity of embedded systems," in *Proc. 4th Int. Conf. Electron., Commun. Aerosp. Technol. (ICECA)*, Nov. 2020, pp. 210–215.

[27] J. Wang, W. Gu, W. Qi, C. Li, D. Chen, G. Adedokun, L. Xu, and F. Wu, "A fully integrated gas detection system with programmable heating voltage and digital output rate for gas sensor array," *IEEE Sensors J.*, vol. 21, no. 5, pp. 6821–6829, Mar. 2021.

[28] A. De Marcellis, G. Ferri, and P. Mantenuto, "Uncalibrated operational amplifier-based sensor interface for capacitive/resistive sensor applications," *IET Circuits, Devices Syst.*, vol. 9, no. 4, pp. 249–255, Jul. 2015.

[29] Z. Tang, Y. Fang, X.-P. Yu, Z. Shi, L. Lin, and N. N. Tan, "A dynamic-biased resistor-based CMOS temperature sensor with a duty-cycle-modulated output," *IEEE Trans. Circuits Syst. II, Exp. Briefs*, vol. 67, no. 9, pp. 1504–1508, Sep. 2020.

[30] S. Pettinato, A. Orsini, and S. Salvatori, "Compact current reference circuits with low temperature drift and high compliance voltage," *Sensors*, vol. 20, no. 15, p. 4180, Jul. 2020.

[31] S. Pan and K. A. A. Makinwa, *Resistor-Based Temperature Sensors in CMOS Technology*, 1st ed. Cham, Switzerland: Springer, 2022.

[32] H. G. Moon, Y. Jung, B. Shin, Y. G. Song, J. H. Kim, T. Lee, S. Lee, S. C. Jun, R. B. Kaner, C. Kang, and C. Kim, "On-chip chemiresistive sensor array for on-road NO_x monitoring with quantification," *Adv. Sci.*, vol. 7, no. 22, Nov. 2020, Art. no. 2002014.

[33] X. Zhu, H. Zhang, and J. Wu, "Chemiresistive ionogel sensor array for the detection and discrimination of volatile organic vapor," *Sens. Actuators B, Chem.*, vol. 202, pp. 105–113, Oct. 2014.

[34] N. Marchand, T. Walewyns, D. Lahem, M. Debliquy, and L. A. Francis, "Ultra-low-power chemiresistive microsensor array in a back-end CMOS process towards selective volatile compounds detection and IoT applications," in *Proc. ISOCS/IEEE Int. Symp. Olfaction Electron. Nose (ISOEN)*, May 2017, pp. 1–3.

[35] S. W. Chiu and K. T. Tang, "Towards a chemiresistive sensor-integrated electronic nose: A review," *Sensors*, vol. 13, no. 10, pp. 14214–14247, Oct. 2013.

[36] A. D. Wilson and M. Baietto, "Applications and advances in electronic-nose technologies," *Sensors*, vol. 9, no. 7, pp. 5099–5148, Jan. 2009.

[37] X. D. Cao, H. Chen, X. Gu, B. Liu, W. Wang, Y. Cao, F. Wu, and C. Zhou, "Screen printing as a scalable and low-cost approach for rigid and flexible thin-film transistors using separated carbon nanotubes," *ACS Nano*, vol. 8, no. 12, pp. 12769–12776, Dec. 2014.

[38] T. Pandhi, A. Chandnani, H. Subbaraman, and D. Estrada, "A review of inkjet printed graphene and carbon nanotubes based gas sensors," *Sensors*, vol. 20, no. 19, p. 5642, Oct. 2020.

[39] M. Hartwig, R. Zichner, and Y. Joseph, "Inkjet-printed wireless chemiresistive sensors—A review," *Chemosensors*, vol. 6, no. 4, p. 66, Dec. 2018.

[40] *PSoC5LP Datasheet*. Accessed: Apr. 7, 2022. [Online]. Available: https://www.infineon.com/dgdl/Infineon-PSoC_5LP_CY8C58LP_Family_Datasheet_Programmable_System-on-Chip_(PSoC_)-DataSheet-v15_00-EN.pdf?fileId=8ac78c8c7d0d8da4017d0ec547013ab9

[41] *DPOT Datasheet*. Accessed: Apr. 7, 2022. [Online]. Available: https://www.analog.com/media/en/technical-documentation/data-sheets/ad5241_5242.pdf

[42] *OPAMP Datasheet*. Accessed: Apr. 7, 2022. [Online]. Available: https://www.ti.com/product/OPA2376

[43] *ADC Datasheet*. Accessed: Apr. 7, 2022. [Online]. Available: https://www.analog.com/en/products/ltc1859.html

SHANTHALA LAKSHMINARAYANA (Graduate Student Member, IEEE) received the B.E. degree in electronics engineering and the M. Tech. degree in VLSI and embedded systems from Visvesvaraya Technological University, Karnataka, India, in 2015 and 2017, respectively. She is currently pursuing the Ph.D. degree with the Department of Electrical Engineering, University of Texas at Arlington, TX, USA. She was a Digital Design Engineer at Intel Technologies India Pvt. Ltd., Karnataka, from 2017 to 2018. Her research interests include sensing embedded systems and CMOS sensing system on a chip.

YOUNGHUN PARK received the B.S. and M.S. degrees in mechanical engineering from Kyung Hee University, Yongin, South Korea, in 2017 and in 2019, respectively. He is currently pursuing the Ph.D. degree with the Department of Electrical Engineering, University of Texas at Arlington, TX, USA. His research interests include sensing embedded systems, mobile app, graphic user interface, and machine learning.

HYUSIM PARK received the B.S. and M.S. degrees in electronics engineering from Kyung Hee University, Yongin, South Korea, in 2014 and 2016, respectively, and the Ph.D. degree in electrical engineering from the University of Texas at Arlington, Arlington, TX, USA, in 2021. Currently, she is a Postdoctoral Researcher with the Department of Electrical Engineering, University of Texas at Arlington. Her research interests include embedded system design and system on a CMOS IC chip for electrochemical sensing application.

SUNGYONG JUNG (Senior Member, IEEE) received the B.S. and M.S. degrees in electronics engineering from Yeungnam University, Kyeongsan, South Korea, in 1991 and 1993, respectively, and the Ph.D. degree in electrical engineering from the Georgia Institute of Technology, Atlanta, GA, USA, in 2002.

He was an Advanced Circuit Engineer at Quellan Inc., Atlanta, from 2001 to 2002. Currently, he is an Associate Professor with the Department of Electrical Engineering, University of Texas at Arlington. His research interests include IC and system design for chemical/bio-applications, system design for precision agriculture, RF IC and system design for wireless communications and radar applications, high-speed CMOS analog and mixed-signal circuit design, and optoelectronic IC design.